Title

THE ROLE OF COMPOUND NUCLEI AND DEEP-INELASTIC SCATTERING IN COMPLEX FRAGMENT PRODUCTION AT INTERMEDIATE ENERGIES

Permalink

https://escholarship.org/uc/item/78s11289

Authors

Wozniak, G.J.
Colonna, N.
Charity, R.J.

Publication Date

1989-02-01

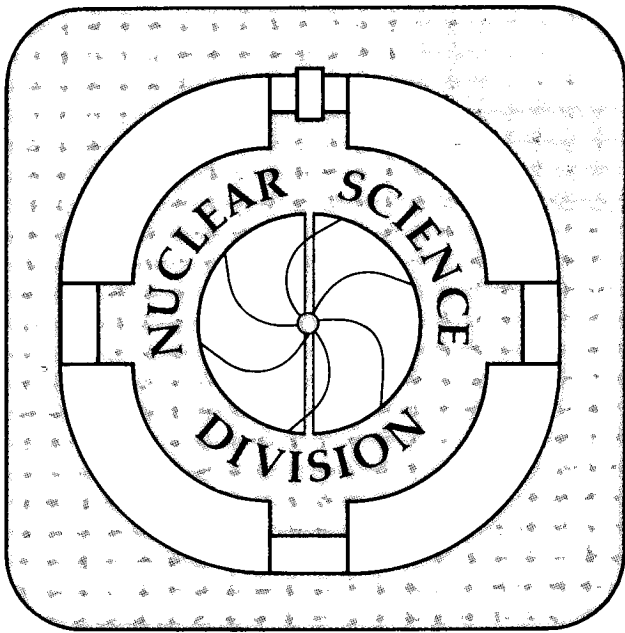# Lawrence Berkeley Laboratory

UNIVERSITY OF CALIFORNIA

Presented at the XII Nuclear Physics Symposium,
Oaxtepec, Mexico, January 3–6, 1989

The Role of Compound Nuclei and Deep-Inelastic Scattering in Complex Fragment Production at Intermediate Energies

G.J. Wozniak, N. Colonna, R.J. Charity, and L.G. Moretto

February 1989

DISCLAIMER

THE ROLE OF COMPOUND NUCLEI & DEEP-INELASTIC SCATTERING IN COMPLEX FRAGMENT PRODUCTION AT INTERMEDIATE ENERGIES

G. J. Wozniak, N. Colonna, R. J. Charity, and L. G. Moretto

Nuclear Science Division, Lawrence Berkeley Laboratory, 1 Cyclotron Rd., Berkeley, California 94720, USA

ABSTRACT

The dependence of complex fragment production on the asymmetry of the entrance channel has been investigated with the 18 A MeV ^{139}La + ^{12}C, ^{27}Al, ^{64}Ni reactions. Invariant cross section plots show a very simple pattern for the two lighter targets and a more complex one for the heavier ^{64}Ni target. The observed complex fragments are shown to result from quasi-elastic/deep-inelastic reactions and from compound nuclei formed in complete/incomplete fusion processes.

1. INTRODUCTION

Complex fragment production has been extensively investigated and debated over the last decade. At low bombarding energies (<10 A MeV), quasi-elastic and deep-inelastic reactions are perhaps the most common sources of complex fragments. In these processes the fragments are produced as the binary decay products of transient dinuclear structures originating from the target-projectile combination. This dinuclear structure, or dinuclear complex diffuses along the mass asymmetry coordinate. The longer the interaction time, the deeper is the energy relaxation, the more isotropic the angular distribution and the broader the product distribution in mass asymmetry.[1,2] At intermediate energies this process is also well established for heavy symmetric systems[3] like ^{100}Mo + ^{100}Mo at 23.4 A MeV. Recently, it has been shown that binary quasi- and deep-inelastic reactions are observed for the more asymmetric 27 A MeV ^{40}Ar + ^{nat}Ag reaction.[4]

It has recently been shown that complex fragments can be emitted by compound nuclei (CN) in a statistical binary decay.[5] This process is best understood by considering the ordinary light particle evaporation and fission as the extreme forms of a common process, whose underlying connection is provided by the mass-asymmetry coordinate. The modulation of the potential energy along the mass-asymmetry coordinate is responsible for the strong variation of the cross sections with mass asymmetry. The relationship between the yield Y and the potential energy V_z is approximately T $\propto$ exp$[-V_z/T]$ where T is the temperature. As the temperature increases, the yield increases dramatically.

At intermediate energies, very hot CN can be formed by incomplete as well as complete fusion reactions. These hot CN can emit copius quantities of complex fragments. The spectator from the incomplete fusion process introduces an additional source of complex fragments. However, both quasi-elastic/deep-inelastic scattering and the spectators in incomplete-fusion produce fragments which are target and/or projectile related.

How can these sources be distinguished? We have found that very asymmetric target-projectile combinations and reverse kinematics are particularly useful for several reasons. 1) The
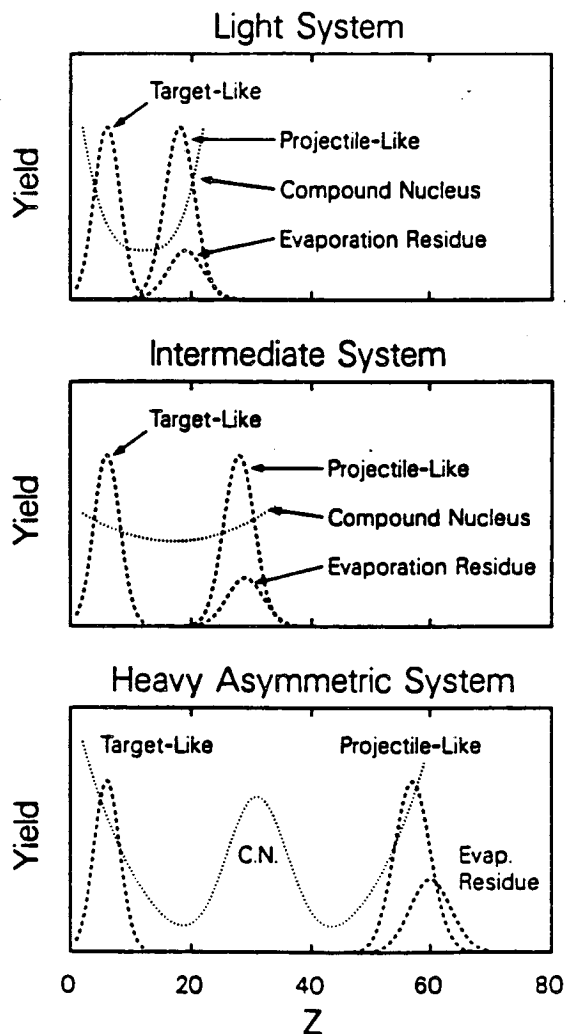

Fig. 1 Schematic diagram showing the contributions from different reaction processes as a function of the product Z-value in a reverse-kinematics heavy-ion reaction for a light, medium and heavy system.

quasi-elastic/deep-inelastic processes are confined to both low and high Z-values (see Fig. 1), whereas the incomplete-fusion spectators are confined to low Z-values leaving the intermediate Z-range uncontaminated for CN products. 2) The limited range of impact parameters leads to a correspondingly narrow range of momentum transfers and consequently to a small range of source velocities. 3) Reverse kinematics brings all the

fragments into a relatively narrow forward cone and boosts their energy, greatly simplifying their detection and identification.

2. VERY ASYMMETRIC ENTRANCE CHANNELS

The evidence of the CN origin of these fragments can be seen in Fig. 2, where the cross section in the $v_{||}$ - $v_\perp$ plane is shown for the 18 A MeV ^{139}La + ^{12}C reaction. For each Z-value, one sees a well defined Coulomb circle. The signature of a binary decay is not only the presence of a sharp Coulomb circle, but the fact that its radius decreases with increasing Z value as required by momentum conservation. The large cross sections observed at low Z values and attached to the low velocity branch are associated with quasi-elastic and deep-inelastic products. The more symmetric the target-projectile combination
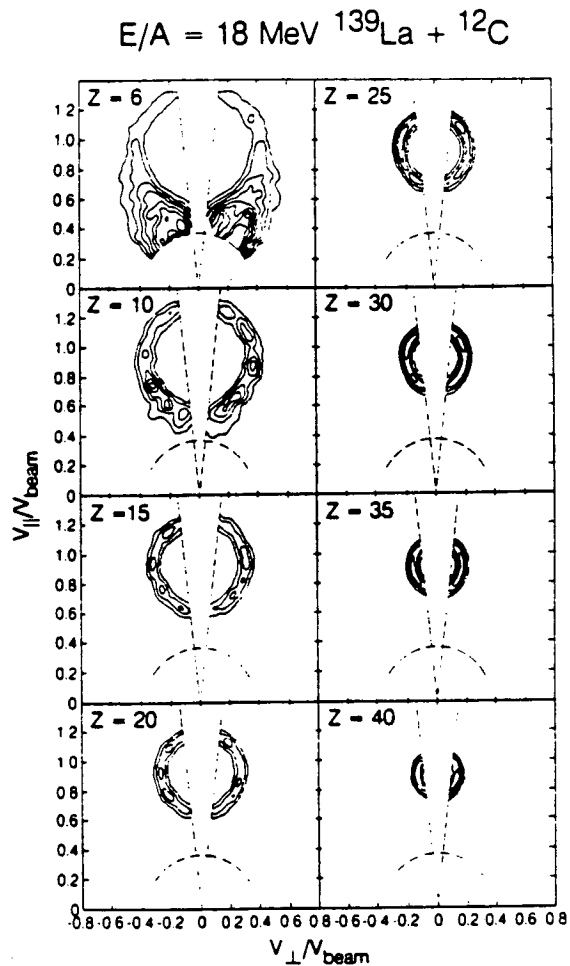
E/A = 18 MeV ^{139}La + ^{12}C

Fig. 2 Contours of the experimental cross section $\partial^2\sigma/\partial v_{||}\partial v_\perp$ in the $v_{||}$ - $v_\perp$ plane for representative fragment Z-values detected in the reaction 18.0 A MeV ^{139}La + ^{12}C. The beam direction is vertical. The dashed lines show the maximum and minimum angular thresholds and the low velocity threshold of the detectors. The magnitudes of the contour levels indicated are relative.

is, the more the CN component is obscured by quasi-elastic & deep-inelastic fragments (see Fig. 1). By making the entrance channel very asymmetric, one minimizes the overlap between the quasi-elastic & deep-elastic products and the binary decay products from a CN.

The centers of the circles give the source velocities which are remarkably independent of the fragment Z value and correspond to nearly complete (Fig. 3) fusion of the light ^{12}C & ^{27}Al targets with the heavy ^{139}La projectile. The nearly linear dependence of the radii of the circles on the fragment Z-value is well reproduced by a simple sphere-spheroid calculation, which demonstrates their Coulomb origin (Fig. 3).
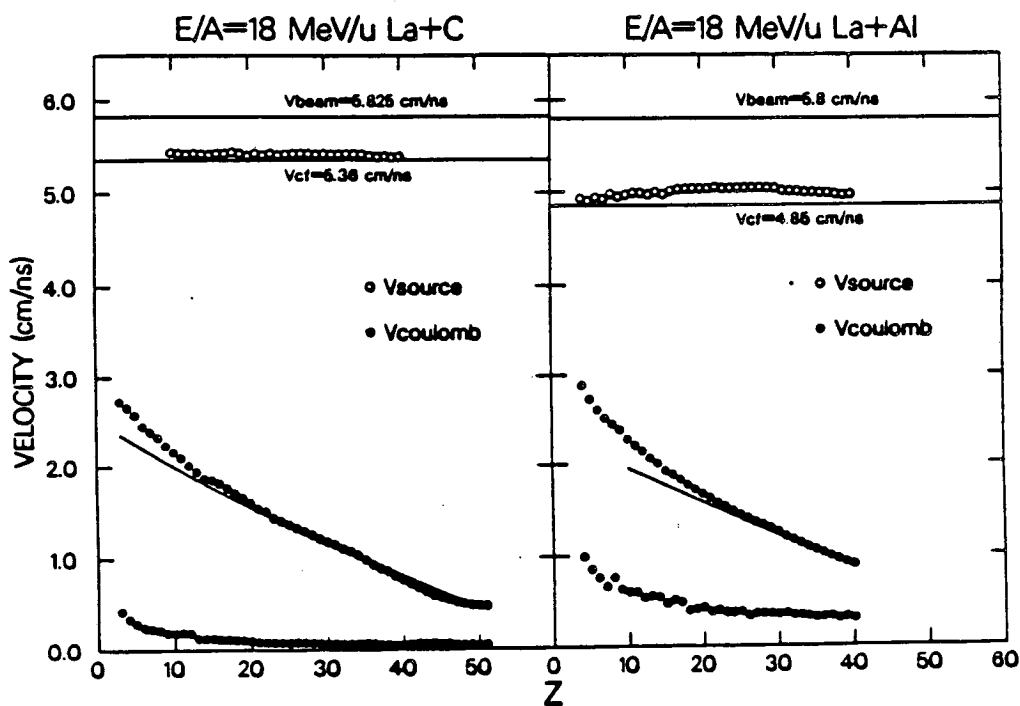
Fig. 3   Source and c.m. velocities extracted from the Coulomb ring of each Z-species produced in the 18 A MeV ^{139}La + ^{12}C, ^{27}Al reactions. See Fig. 2. The velocities corresponding to the beam and complete fusion are shown as shown as horizontal lines. The Coulomb velocities are well reproduced by a simple sphere-spheroid calculation (solid curve).

For compound nucleus emission, the most important feature of the angular distributions is their symmetry about 90° in the center-of-mass frame. Because of the

large angular momenta involved in these reactions, one also expects the angular distributions to be of the form $d\sigma/d\Omega = 1/\sin\theta$ or $d\sigma/d\theta = $ constant. This would correspond to an isotropic distribution along the Coulomb rings. In contrast, the angular distributions of projectile-like and target-like fragments produced in quasi- or deep-inelastic processes should show a backward and a forward peaking, respectively.

The angular distributions for the 18 A MeV ^{139}La + ^{12}C, ^{27}Al reactions are shown in Fig. 4. In general, one observes angular distributions that are flat ($d\sigma/d\theta = $ constant),

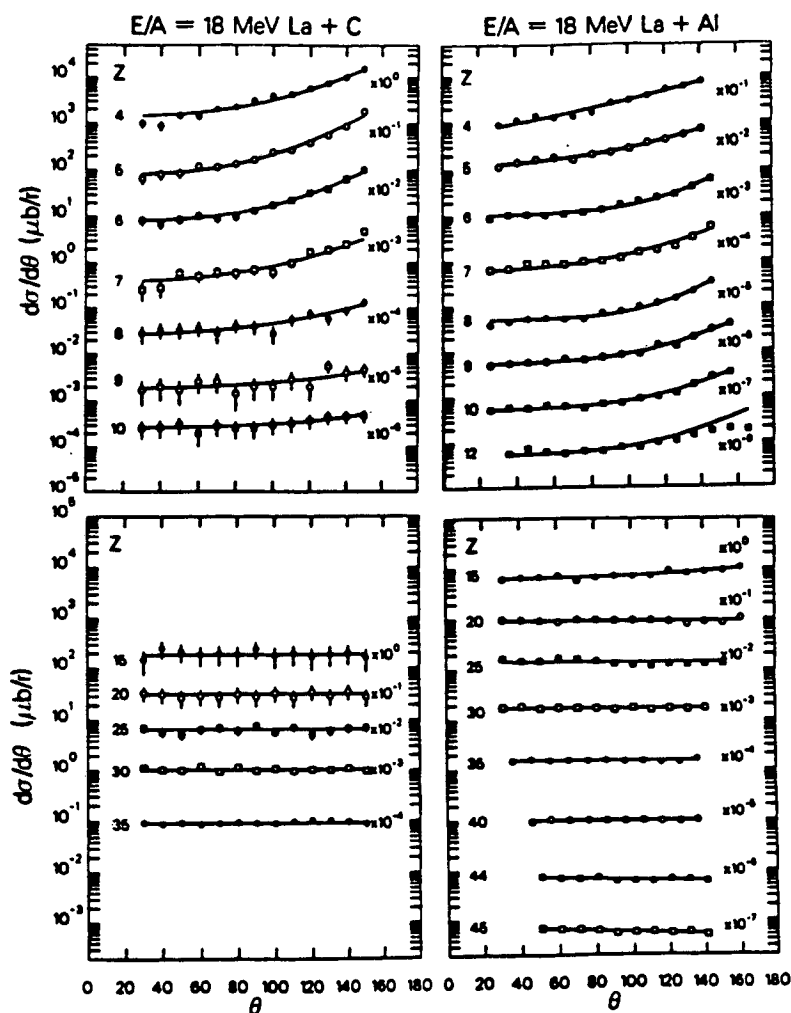
Fig. 4 Angular distributions ($d\sigma/d\theta$) in the source frame for representative Z values from the 18 A MeV ^{139}La + ^{12}C, ^{27}Al reactions. The backward rise at low Z values is attributed to target-like and projectile-like quasi and deep inelastic products. Note that the cross sections are flat for a large range of Z values intermediate between the target and the projectile.

except in the vicinity of the target or projectile Z value, where quasi-elastic, deep-inelastic and target-spectator fragments manifest themselves with a forward or backward peaking.

For the ^{12}C target, the backward peaking of the target-like fragment is most prominent for Z = 4, 5, 6 and vanishes for Z ≥ 10. In the case of ^{27}Al target, the backward peak extends up to Z = 13, due to the larger atomic number of the target. Thus the use of a heavier target tends to mask the CN component with quasi- and deep-inelastic products for a larger number of products. In the same figure, one also observes a forward peaking associated with the heaviest fragments (projectile-like) from the $^{139}La + ^{27}Al$ reaction.

The cross sections, and their dependence upon energy and fragment Z-value are of particular importance to demonstrate their CN origin. When a CN is about to decay, it has many exit channels which will be chosen proportionally to their associated phase space. In particular, neutron, proton, and alpha-particle decays, because of their small barriers, are the dominant decay channels with which complex fragments must compete. Thus, the cross section associated with the emission of any given fragment should reflect this competition. A schematic picture of the statistical decay of an A =

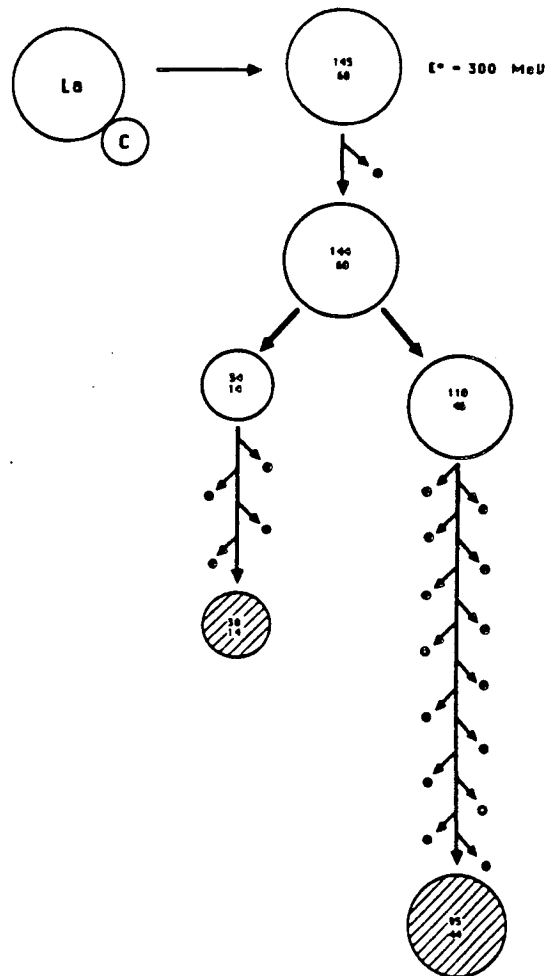Fig. 5 An example of the production of 2-body event from the sequential decay of the compound nucleus ^{145}Eu (ℓ_{max} = 60 ħ, at 300 MeV excitation energy) as calculated by the statistical model code GEMINI. Evaporated neutrons and light charged particles (Z ≤2) are shown by the filled and open circles, respectively. Residue nuclei and complex fragments are labelled by their mass and charge numbers.

145 nucleus, with 300 MeV of excitation energy is shown in Fig. 5. For this decay chain, the hot nucleus first emits a neutron, then splits into two large hot fragments, which cool by emitting a large number of n's, and a few light charged particles. In Fig. 6 the measured and calculated absolute charge distributions are compared for the 18 A MeV ^{139}La + ^{12}C reaction. The calculations were performed with the CN decay code (GEMINI)[7], which follows the decay of the CN through all the channels including complex fragment emission. The code accurately reproduces the shape, magnitude, charge and energy dependence of the absolute cross sections, confirming CN decay as the dominant mechanism for this system.
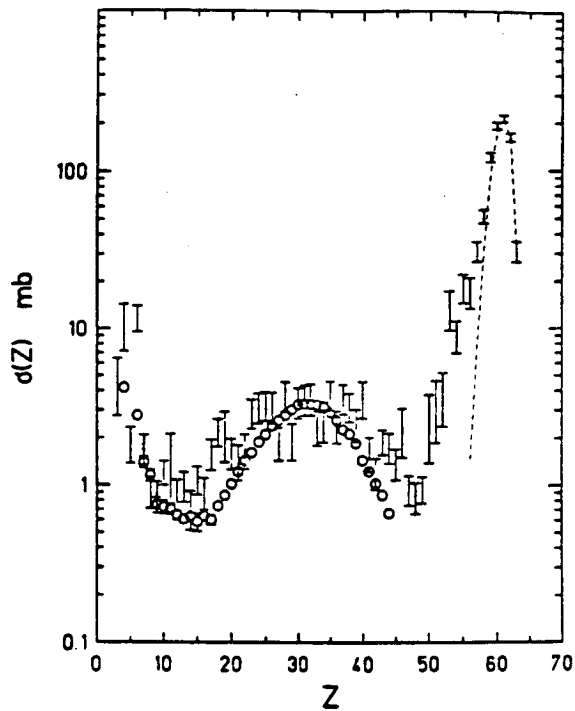

Fig. 6 Comparison of experimental and calculated charge distributions for the ^{139}La + ^{12}C reaction at E/A = 18.0. The experimental data are indicated by the hollow circles and the values calculated (E* = 188 MeV, J_{max} = 55ħ) with the code GEMINI are shown by the error bars. The dashed curve indicates the cross section associated with classical evaporation residues which decay only by the emission of light particles (Z ≤ 2).

Coincidence data confirm the binary nature of the decay. The Z_1 - Z_2 scatter plots show a diagonal band characteristic of a binary decay. The spectrum associated with the sum Z_1 + Z_2 shows a rather sharp peak very near the value of Z_{total} indicating that there is only a small charge loss and that most (95%) of the total charge available in the entrance channel is found in the two exit-channel partners.

In summary, very asymmetric target-projectile combinations lead to the formation of a simple source pattern, a circular Coulomb ring, easily identifiable in reverse kinematics. These reactions have led to the identification of the CN as an important source of complex fragments formed in binary decays at all exit channel asymmetries, and of quasi- and

deep-inelastic processes as responsible for fragment production in the vicinity of the target and projectile. At low bombarding energy, CN are formed in complete fusion reactions. At higher energies, they are formed in incomplete fusion reactions.

3. MORE SYMMETRIC ENTRANCE CHANNELS

More symmetric entrance channels appear to be more complicated and the lack of simple source patterns has led to a lot of discussions regarding their origin. The complexity of these reactions seems to arise from the fact that their mechanism depends as much on the mass asymmetry of the entrance channel as on the bombarding energy. If for more symmetric systems, CN are formed in both complete and incomplete fusion processes, then there should be a continuum of sources corresponding to different impact parameters. These sources would have a continuum of velocities, total masses, and excitation energies, but in all other respects they would resemble CN formed in the complete fusion of more asymmetric systems, and decay in a similar way.

To investigate the above scenario, we have studied the reaction $^{139}La + {}^{64}Ni$ at 18 A MeV and determined the velocity distribution, mass and excitation energy of the sources. In this experiment the mass of a fragment was inferred from its measured charge as described in Ref. 6. The velocity of a fragment was calculated from its measured energy and calculated mass. The velocity plots for inclusive products from the ^{64}Ni target are very complicated in contrast to the simple ones observed for the ^{12}C & ^{27}Al targets. These inclusive data do not lend themselves to a ready interpretation and thus we turn to the coincidence data.

For binary coincidences in which one fragment has the atomic number $Z = 30$, the cross section $\partial^2\sigma/\partial v_{||}\partial v_{\perp}$ in the $v_{||} - v_{\perp}$ plane is shown in Fig. 7b. For the $^{139}La + {}^{64}Ni$ reaction, one observes an elliptical pattern stretched along the beam direction. Although a high degree of relaxation can be inferred, it is not possible to associate these fragments with a single source. For comparison, a more asymmetric reaction like $^{139}La + {}^{12}C$ (see
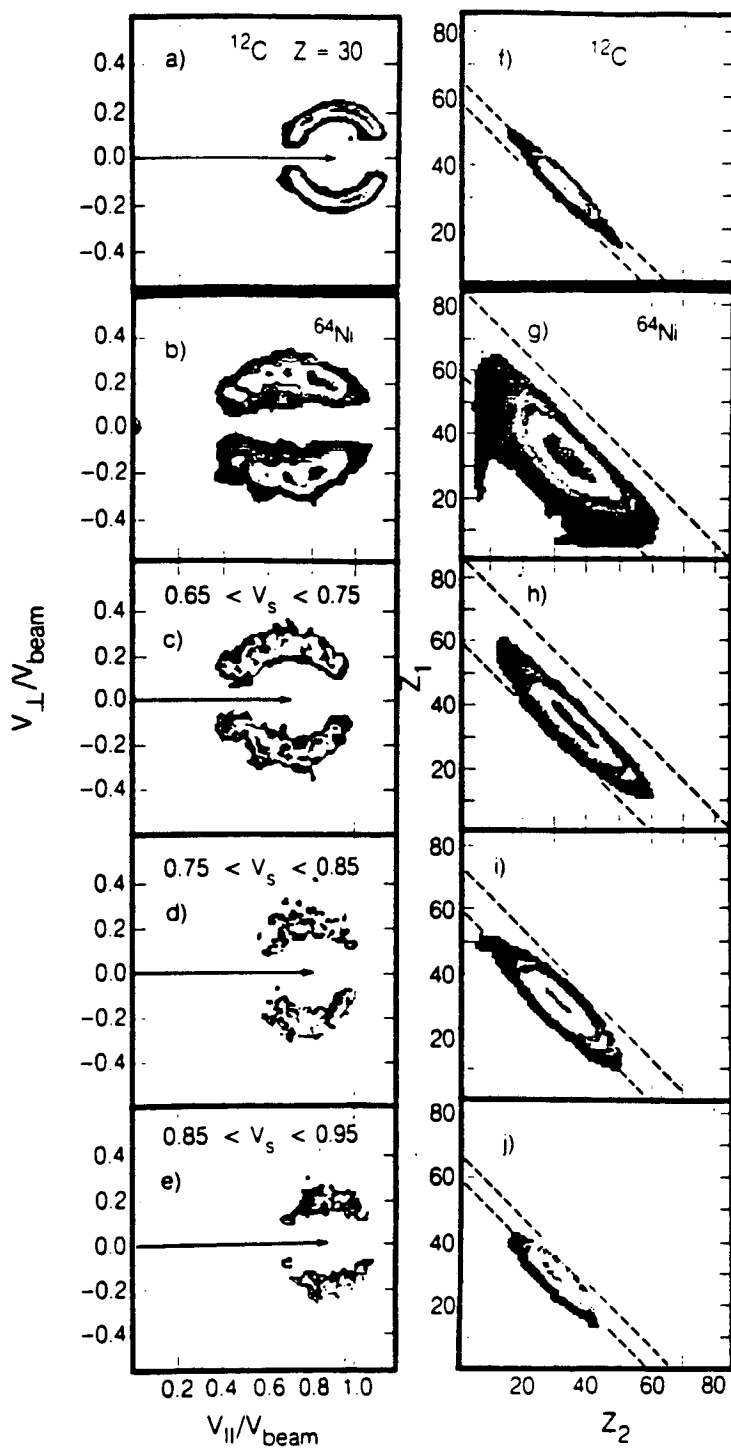
Fig. 7   Contour diagrams of invariant cross section in the $V_{\parallel}$ - $V_{\perp}$ plane (left column) and Z_1 - Z_2 (right column) for Z = 30 fragments from the 18 A MeV ^{139}La + ^{12}C reaction (first row) and for the 18 A MeV ^{139}La + ^{64}Ni reaction. Various gating conditions on the source velocity are indicated to the left of each row. The horizontal arrows indicate the magnitude of the source velocity and the diagonal dashed lines indicate the atomic numbers of the projectile and the fused system.

Fig. 7a) shows a sharp isotropic Coulomb circle indicating the presence of a single source with a well defined velocity. The Z_1-Z_2 correlation diagram for the ^{139}La + ^{64}Ni reaction (Fig. 7g) is very broad whereas the one for the ^{139}La + ^{12}C reaction is much narrower.

These "anomalous" features become understood when the velocity spectrum of the centers of mass of the two coincidence fragments is determined. This spectrum is shown in Fig. 8 for the three reactions 18 A MeV ^{139}La + ^{12}C, ^{27}Al and ^{64}Ni. For the very asymmetric ^{139}La + ^{12}C , ^{27}Al systems, the corresponding spectrum shows a single sharp peak. This peak corresponds to the velocity of the center-of-mass of the entire system and indicates the absence of a third body. The total relaxation of the kinetic energy, mass, and angular distributions, permits us to attribute these peaks to a complete fusion process. For the more symmetric ^{139}La + ^{64}Ni reaction, one observes a similar peak that can be attributed to complete fusion plus an additional shoulder that stretches out to velocities approaching that of the projectile. This high velocity shoulder indicates the presence of a third body associated with a continuum of incomplete fusion processes extending over the entire allowed mass range. Of course, caution must be exercised in interpreting this curve as the distribution in source velocities. On the one hand, the peak can contain all kinds of two body decays, in particular deep-inelastic decay. On the other, the measured distribution may be biased (though not seriously) by
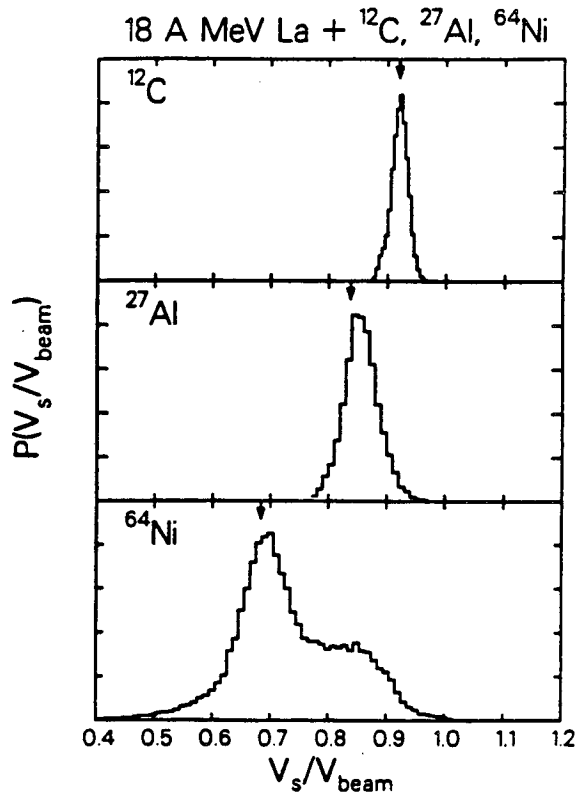

Fig. 8 Source velocity distribution for the 18 A MeV ^{139}La + ^{12}C, ^{27}Al, ^{64}Ni reactions as extracted from the binary coincidences (see text). The vertical arrows indicate the velocities corresponding to complete fusion for the three reactions.

the coincidence efficiency of our apparatus, and the velocity spectrum is broadened by the light particle evaporation, which may either precede or follow the complex fragment decay.

Despite these possible biases, the measured source velocity distribution can be used to unravel the complexity of the $^{139}La + ^{64}Ni$ reaction by selecting events with well defined source velocities. For example, in Fig. 7(c, d, & e), the velocity plots are shown, for Z = 30, but gated on three different velocity bins, namely the velocity corresponding to complete fusion velocity, 50% fusion and 25% fusion. These three velocity plots now display isotropic circular patterns similar to the Coulomb circles seen in the very asymmetric systems, but with their centers progessively shifted towards higher values of $v_{||}$. There is also a striking decrease in the radii of these Coulomb circles with increasing source velocity. This correlation occurs since, as the projectile picks up more mass from the target, its velocity decreases. The complex fragment is thus emitted from a heavier and slower source. In addition, as the total charge of the source decreases, the Coulomb velocity associated with a fixed fragment Z value decreases, because the splitting becomes more symmetric.

The ungated Z_1-Z_2 correlation diagram as well as those gated on the same velocity bins are also shown in Fig. 7. The broad ungated distribution (see Fig. 7g) indicates a broad distribution in the total charge of the source due to the extended range of incomplete fusion. By restricting the source velocity, this broad distribution is decomposed into three narrower correlation diagrams (see Figs. 7h, i, j), with the characteristic diagonal pattern observed for very asymmetric systems like $^{139}La + ^{12}C$ (see Fig. 7f). As the source velocity increases, the diagonal pattern shifts from larger to smaller total Z values. The largest average sum of the fragment atomic numbers $<Z_1 + Z_2>$ occurs for the complete fusion velocity. The quantity $<Z_1 + Z_2>$ decreases with increasing source velocity, which corresponds to progressively less extensive fusion of the target with the projectile. Thus, the broad ungated correlation diagram observed in Fig. 7g, can be

decomposed into a series of narrower patterns, by setting gates on the source velocity.

The observed atomic numbers of the coincident fragments are those resulting after evaporation from either the hot CN, or the hot primary fragments resulting from its binary decay. It would be useful to obtain information on their primary atomic numbers. One can estimate the total primary charge of the incomplete fusion product from the corresponding source velocity, namely:

$$Z_{IF} \cong Z_P V_P/V_{IF} . \tag{1}$$

Similarly, one can estimate the excitation energy of the incomplete fusion product:

$$E_x (IF) \cong E_x (CF) \frac{V_P - V_{IF}}{V_P - V_{CF}} . \tag{2}$$

For complete fusion, one obtains $E_x \sim 800$ MeV for the compound nucleus ^{205}At, which corresponds to 4 MeV/nucleon and a temperature of 6.5 MeV. While higher temperatures have been advocated from spectral slopes or particle multiplicities, this may well be the highest temperature that can be firmly associated with a well characterized system.

One should be aware that light particle evaporation causes some uncertainty in these estimated quantities. With this caution in mind, one can plot the difference between the estimated primary charge and the measured average secondary charge as a function of the estimated excitation
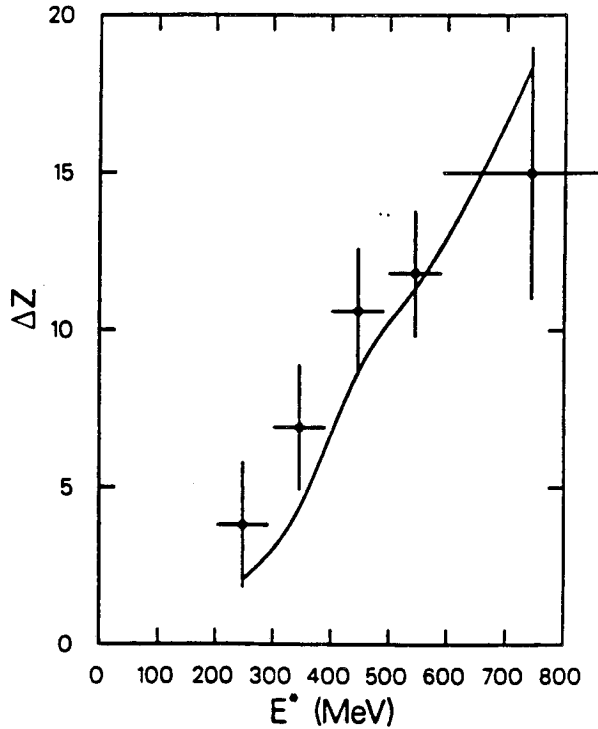

Fig. 9 The measured evaporated charge (dots) plotted versus the excitation energy determined from the source velocities for the 18 A MeV ^{139}La + ^{64}Ni reaction. The horizontal and vertical bars on each data point reflect the width of the bin in the source velocity from which the primary charge and the excitation energy of the incomplete fusion product was extracted.

energy (see Fig. 9). The approximate linearity of the plot is consistent with the evaporation hypothesis. A more quantitative check can be made by assuming that the binary decay occurs first and that all of the remaining excitation energy is disposed of by evaporation from the two fragments. The maximum partial wave leading to complete fusion was calculated with the Bass model[8], while in the case of incomplete fusion the model of Ref. 9 was used. The angular momentum of the fragment, needed for the evaporation calculation, was estimated from a two sphere scission configuration.

The results obtained from the evaporation code PACE are also shown in Fig. 9. Given the very rough assumptions of equations 1 & 2 and the crude estimate of the angular momentum of the fragments, the agreement between the data and the calculations is quite satisfactory.
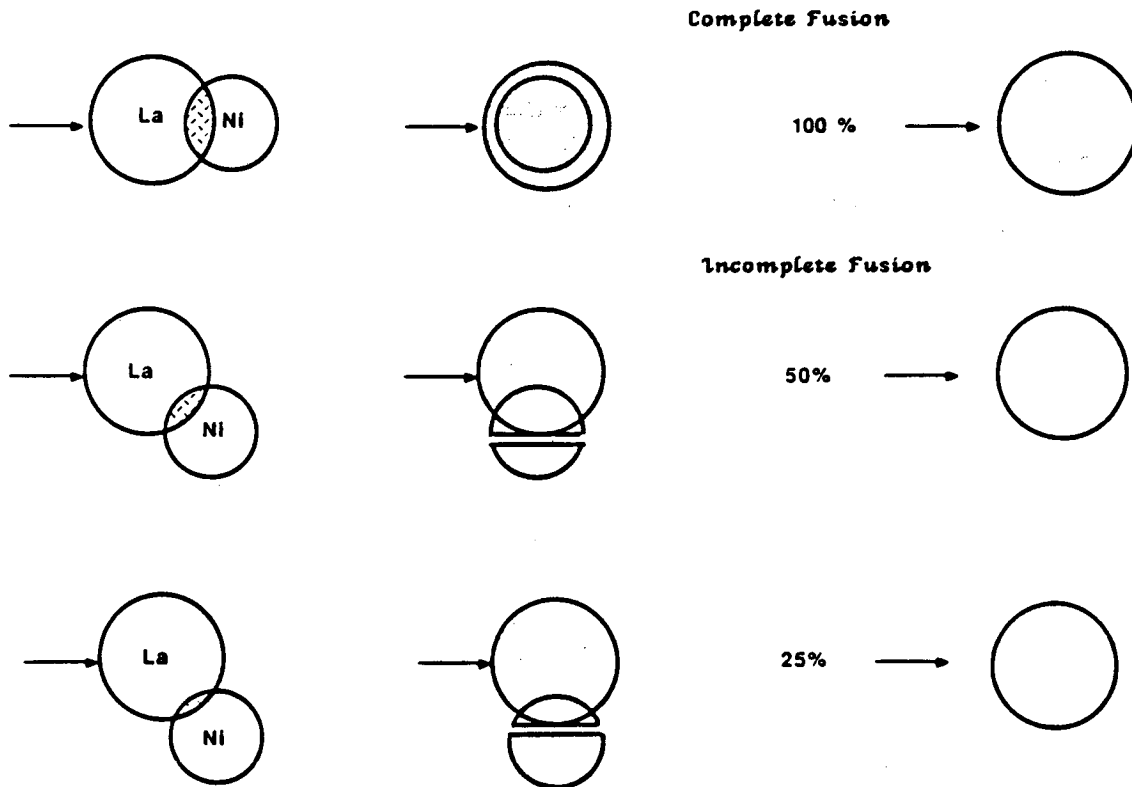

Fig. 10 Schematic diagram illustrating the massive transfer picture.

In light of the above discussion, we can describe the 18 A MeV ^{139}La + ^{64}Ni reaction as shown schematically in Fig. 10. The events associated with the "complete fusion peak" arise from either compound nucleus binary decay of the complete fusion object, or from quasifission binary decay, or, from (quasi) deep inelastic reactions. 2) The events associated with the higher velocity components are essentially ternary incomplete fusion events. The target-like spectator, observable in singles[5] as part of the low velocity "big foot" is not detected in coincidence. The forward moving incomplete fusion products, whose masses are smaller the faster their velocities, give rise to the observed continuum of complex fragment sources. 3) If the incomplete fusion product undergoes a binary decay, this continuum can be analyzed by reconstructing the source velocity from the two coincident heavy fragments.

From the analysis of the present more symmetric system, we conclude that the processes involved in complex fragment formation, in this energy regime, are no different than those present in more asymmetric systems. The only complicating feature is the broad range of incompete fusion products, resulting in a broad range of source velocities. Perhaps this conclusion will apply for symmetric systems and even higher bombarding energies. In any event, this novel technique allows one to study, in a single reaction system, the decay properties of a wide range of compound nuclei with a continuous range of excitation energies.

ACKNOWLEDGEMENTS

REFERENCES

1. Schröder, W. U. and Huizenga, J. R., Ann. Rev. Nucl. Sci. **27**, 465 (1977).
2. Moretto, L. G. and Schmitt, R. P., J. Phys. **37C5**, 109 (1976).
3. Olmi, A. et al., Europhys. Lett. **4**, 1121 (1987).
4. Boderie, B. et al., Phys. Lett. **205**, 26 (1988).
5. Moretto, L. G. and Wozniak, G. J., Prog. in Part. & Nucl. Phys. **21**, 401 (1988) and references therein.
6. Charity, R. J. et al., Nucl. Phys. **A483**, 371 (1988).
7. Charity, R. J. et al., Nucl. Phys. **A476**, 516 (1988).
8. Bass, R., Phys. Rev. Lett. **39**, 265 (1977).
9. Moretto, L. G. and Bowman, D. R., Proc. of the XXIV Int'l Winter Meeting on Nucl. Phys., Bormio, Italy, Jan. 20 -25, 1986, Ricerca Scientifica ed. Educazione Permanente, Suppl. N. <u>49</u>, 126 (1986).